Society For Biomaterials

Tailored magnetic nanoparticles for optimizing magnetic fluid hyperthermia

Amit P. Khandhar,[1] R. Matthew Ferguson,[1] Julian A. Simon,[2] Kannan M. Krishnan[1]

[1]Department of Materials Science & Engineering, University of Washington, Materials Science and Engineering, Seattle, Washington 98195

[2]Fred Hutchinson Cancer Research Center, Division of Clinical Research, Seattle, Washington

Received 5 April 2011; revised 23 September 2011; accepted 21 October 2011

Published online 30 December 2011 in Wiley Online Library (wileyonlinelibrary.com). DOI: 10.1002/jbm.a.34011

Abstract: Magnetic Fluid Hyperthermia (MFH) is a promising approach towards adjuvant cancer therapy that is based on the localized heating of tumors using the relaxation losses of iron oxide magnetic nanoparticles (MNPs) in alternating magnetic fields (AMF). In this study, we demonstrate optimization of MFH by tailoring MNP size to an applied AMF frequency. Unlike conventional aqueous synthesis routes, we use organic synthesis routes that offer precise control over MNP size (diameter ~10 to 25 nm), size distribution, and phase purity. Furthermore, the particles are successfully transferred to the aqueous phase using a biocompatible amphiphilic polymer, and demonstrate long-term shelf life. A rigorous characterization protocol ensures that the water-stable MNPs meet all the critical requirements: (1) uniform shape and monodispersity, (2) phase purity, (3) stable magnetic properties approaching that of the bulk, (4) colloidal stability, (5) substantial shelf life, and (6) pose no significant *in vitro* toxicity. Using a dedicated hyperthermia system, we then identified that 16 nm monodisperse MNPs (σ–0.175) respond optimally to our chosen AMF conditions ($f = 373$ kHz, $H_o = 14$ kA/m); however, with a broader size distribution (σ–0.284) the Specific Loss Power (SLP) decreases by 30%. Finally, we show that these tailored MNPs demonstrate maximum hyperthermia efficiency by reducing viability of Jurkat cells *in vitro*, suggesting our optimization translates truthfully to cell populations. In summary, we present a way to intrinsically optimize MFH by tailoring the MNPs to any applied AMF, a required precursor to optimize dose and time of treatment. J Biomed Mater Res Part A: 100A: 728–737, 2012.

Key Words: magnetic fluid hyperthermia, *in vitro* hyperthermia, monodisperse iron oxide magnetic nanoparticles, cytotoxicity

How to cite this article: Khandhar AP, Ferguson RM, Simon JA, Krishnan KM. 2012. Tailored magnetic nanoparticles for optimizing magnetic fluid hyperthermia. J Biomed Mater Res Part A 2012:100A:728–737.

INTRODUCTION

Cancer therapeutics relies heavily on the combination of conventional remedies such as radiation, chemotherapy, and surgical removal of tumors. Recent cancer statistics[1] show declines in new diagnoses (−1.1% AAPC* from 2002 to 2006) and death rates (–1.6% AAPC from 2002 to 2006), primarily due to declines in the most common types of cancer (lung, prostate, breast, and colorectal). From both technological and clinical perspectives, however, vast room for improvement in treatment options still remains.

The adverse side effects from conventional therapies and the resulting patient discomfort have encouraged researchers to explore site-specific therapies with the aid of magnetic nanoparticles (MNPs).[2–6] Furthermore, MNPs also offer diagnostic and therapeutic monitoring with imaging modalities such as Magnetic Resonance Imaging (MRI) and the emerging technique of Magnetic Particle Imaging (MPI).[2,7–9] Since the idea of site-specific therapy is to restrict treatment to the cancer site, thereby minimizing side effects and patient discomfort, MNPs are an attractive option because they can be remotely targeted by application of external magnetic field gradients[10] or other active[4,11,12] and passive[12,13] targeting methods. Once localized, Magnetic Fluid Hyperthermia (MFH), a therapeutic modality that utilizes alternating magnetic fields (AMF) to dissipate heat from the resulting relaxation losses in MNPs, can be used to induce heating.[2,6] Heating cancer cells (typically to ~42 to 43°C) is known to disrupt cellular metabolism making adjuvant therapy by conventional established methods more efficient.[14,15] Thus, hyperthermia is best characterized as a synergistic modality rather than an independent one.[16,17] A wide range of ferromagnetic nanoparticles, including metals/alloys with superior magnetic properties, can be synthesized for MFH.[2,18–21] However, only iron oxide

*AAPC – Average Annual Percentage Change.

Correspondence to: K. M. Krishnan; e-mail: kannanmk@uw.edu

Contract grant sponsors: NIH/NIBIB; contract grant numbers: R21 EB008192, RO1 EB013689

(γ-Fe_2O_3 or Fe_3O_4) MNPs show minimal toxicity[5,22,23] and are FDA approved for MRI contrast agents[24] and more recently for treatment of patients with chronic kidney disease.[25] Furthermore, due to their modest magnetic characteristics[26] when compared to the ferromagnetic elements,[27,28] they require the utmost optimization in terms of their morphological (size, size distribution, shape), crystallographic (phase purity), and magnetic (relaxation) characteristics for effective application in MFH.

MFH has been studied on both *in vitro*[29–32] and *in vivo*[33,34] platforms. However, the difficulty in delivering a sufficient amount of MNPs at the target site in order to promote a noticeable therapeutic outcome is one of the major hurdles impeding clinical adoption of MFH.[2,6] For example, an estimated 32 mW of power dissipation for a treatment time of 10 min is required to raise the temperature of 1 g of prostate tumor tissue (c_P ~3.8 kJ kg^{-1} s^{-1})[35] by 5°C. This is an underestimation and would be significantly higher if cooling from blood perfusion is taken into account. Nevertheless, based on this rough estimate, a minimum dose of 0.32 mg of MNPs that have a Specific Loss Power (SLP) of 100 W g^{-1}, per gram of tumor tissue would be needed to locally raise the temperature by 5°C.

SLP output can be optimized if the effective magnetization relaxation time of MNPs match the applied AMF frequency.[2,6,36–38] The effective relaxation time depends on both Néel (magnetization reversal) and Brownian (particle rotation) time components. Brownian relaxation (τ_B) depends linearly on the fluid viscosity (η) and the hydrodynamic particle volume (V_H), and is typically difficult to control due to the dynamic nature of the *in vivo* environment. It can also be detrimental to SLP output if the hydrodynamic volume is found to increase significantly.[39] On the other hand, the operating Néel relaxation time (τ_N) is far more reliable as it depends exponentially on the product of magnetic anisotropy constant (K) and the magnetic core volume (V_m), i.e. $\tau_N \sim \exp(KV_m)$. The core volume remains constant, irrespective of changes in the hydrodynamic volume and can be tailored to optimize the relaxation time. However, due to this exponential dependence even slight variation in the size distribution dramatically alters the effective relaxation time. It is clear from the above discussion that the effective relaxation time is dependent on the particle volume and this dependence is particularly strong if dominated by the Néel component. Thus, it is crucial to tailor particle size and, more importantly, the size distribution for a chosen AMF frequency, and also ensure MNPs do not agglomerate in biological medium in order to maximize SLP output from Brownian component. For instance, according to a model based on the known size-dependence of magnetic relaxation in MNPs,[37] if size distribution increases from highly monodisperse ($\sigma = 0$, where σ represents the standard deviation of the lognormal distribution) to polydisperse ($\sigma = 0.25$), heating rate degrades by a factor of 5. This changes our estimate above, which assumes ideally monodisperse MNPs, to ~1.6 mg of polydisperse MNPs ($\sigma = 0.25$) per gram of tumor tissue or five times more than needed. The decrease in heating rate is especially dramatic for deviations in the size of MNPs at or near the optimum size, that is size that matches the applied AMF frequency.

Popular MNP synthesis methods typically involve coprecipitation of iron salts in aqueous solution that inherently produce biocompatible particles, but lack the ability to produce monodisperse MNPs.[2,3] So far, most MFH studies utilize MNPs synthesized by such methods, and rely primarily on "extrinsic" augmentations in order to counteract the ineffectiveness of polydisperse MNP dispersions and improve therapeutic efficiency. Such augmentations include, directly injecting tumors with large quantities of MNPs[34] or planting "thermoseeds" at tumor sites.[40] However, in most cases the exact tumor location may be either unknown or require invasive methods to be reached. Increasing the administered MNP dose is also limited by the maximum tolerated dose (MTD); alternatively, increasing the applied magnetic field amplitude is also not an option as it can result in nonspecific eddy current heating of surrounding tissue.[34] Thus, the best approach to optimize MFH is to intrinsically tailor the MNPs, which are the actual source of heating.

To achieve the latter, we have synthesized highly monodisperse magnetite (Fe_3O_4) MNPs using organic methods and subsequently transferred them to aqueous phase using a biocompatible amphiphilic polymer. The organic synthesis route gives exceptional control over size, size distribution, shape, and phase purity, enabling synthesis of MNPs specifically tailored for any chosen AMF frequency. The resulting power output, or SLP, is maximized and optimized for that specific frequency. To confirm that the synthesized MNPs possess the necessary characteristics for optimum MFH performance, we systematically characterized them. A dedicated hyperthermia system was used to measure heating capacity of MNPs and identify the optimum size for our chosen AMF conditions ($f = 373$ kHz, $H_0 = 14$ kA/m). Finally, we compared the *in vitro* therapeutic effectiveness of our monodisperse MNPs to induce hyperthermia in cells as a function of concentration and size.

MATERIALS AND METHODS

Chemicals

Iron (III) Chloride, anhydrous (98%) was purchased from Alfa-Aesar. Oleic acid (tech. grade, 90%), 1-octadecene (tech. grade 90%), poly(maleic anhydride-alt-1-octadecene) or PMAO ($M_n = 30{,}000$–$50{,}000$), methoxy poly(ethylene glycol) ($M_n = 5000$) and were purchased from Sigma-Aldrich.

Synthesis of Fe_3O_4 magnetic nanoparticles

Magnetite MNPs were synthesized according to a procedure based on pyrolysis of metal fatty acid salts; specifically, Fe^{3+}-oleate. Fe^{3+}-oleate was prepared according to previous methods[41–43] and stored as a stock solution (conc. 18 wt %) in 1-octadecene (ODE, technical grade 90%). We have developed a method that allows us to reproducibly synthesize highly monodisperse Fe_3O_4 nanoparticles of diameters ranging from 10 to 25 nm by reacting predefined amounts of Fe^{3+}-oleate and oleic acid (tech. 90%) in ODE. For

instance, synthesis of 15 nm particles required 0.2 mmol/g of Fe^{3+}-oleate and 3 mmol/g of oleic acid in 2.5 g of reaction solvent (ODE). The mixture was refluxed overnight ($\geq$24 h) at 320°C under an argon blanket and vigorous stirring. Ageing 24 h typically resulted in narrow size distribution compared to shorter times ($\sim$12 h), which resulted in relatively broader size distribution. On the basis of this observation, MNPs with different size distributions were synthesized and enabled us to study the effect of size distribution on SLP. Nucleation of nanoparticles was observed as a sudden change in color, from clear to black. The final product was collected and washed to remove excess surfactant and solvent. MNPs were precipitated using an excess of 1:1 (v/v) mixture of chloroform and methanol; they were then separated using a magnet and the washing step was repeated at least four times. MNP powder, obtained by drying in vacuum for 30 min, was coated with oleic acid and could be easily dispersed in organic solvents such as toluene or chloroform. X-ray diffraction (XRD – Rigaku) was routinely used to confirm the crystalline phase of Fe_3O_4 and determine size of nanocrystals. For select samples the Fe_3O_4 phase purity was independently confirmed by more sophisticated fine structure analysis of the Fe $L_{3,2}$ edges in transmission electron energy-loss spectroscopy.[44] A Vibrating Sample Magnetometer (VSM - Lakeshore) was used to measure magnetic properties of the samples.

Synthesis of PMAO-PEG

Methoxy-poly(ethylene glycol) (m-PEG, $M_n = 5000$) was used to PEG-ylate poly(maleic anhydride-alt-1-octadecene (PMAO ($M_n = 30{,}000$-$50{,}000$). PEG is considered highly biocompatible as it rejects nonspecific protein adsorption, is nonimmunogenic and nontoxic.[45] Under acid catalysis, the hydroxyl group on m-PEG forms an ester bond with the anhydride ring on PMAO. In a typical reaction 2 g of PMAO ($\approx$50 μmol) was reacted with 3.75 g of m-PEG ($\approx$750 μmol) in 20 mL of acetone. A few drops of concentrated sulfuric acid were added to catalyze the reaction. The mixture was refluxed at 58°C in an argon atmosphere. After 24 h, the mixture was cooled to room temperature and the polymer was obtained by precipitation in excess DI water. After several more DI water washes by sonication and centrifugation, the white polymer cake was freeze dried for 24 h. The final product was obtained as a white powder and stored at room temperature. Gel Permeation Chromatography (GPC) was used to confirm the increase in molecular weight after PEG-ylation (data not shown).

Phase transfer of hydrophobic MNP using PMAO-PEG

In a typical phase transfer process, about 10 mg of oleic acid coated MNP (MNP@OA) and 10 mg of PMAO-PEG were dissolved in 1–2 mL of chloroform. The mixture was sonicated in an ultrasonic bath for about 15 min and dried under a stream of argon. The dried nanoparticle-polymer complex was dispersed in 1 mL of 1x Tris-acetate-EDTA (TAE) buffer by a 30-min sonication step. MNP coated PMAO-PEG (MNP@PMAO-PEG) were filtered using a 0.45-μm nylon syringe filter. To remove excess unbound polymer, MNP@PMAO-PEG were passed through a Sephacryl™ S-200 HR gel column (GE Healthcare Life Sciences). Either deionized (DI) water or 1x phosphate buffered saline (PBS) was used as the eluent. Nanoparticles were stored at 4°C until further use. Iron concentration was determined using an Inductively Couple Plasma Atomic Emission Spectrophotometer (ICP-AES, Jarrell Ash 955). MNPs were analyzed using transmission electron microscope (TEM–FEI Tecnai™ G2 F20) images to gain a visual perspective and confirm the overall uniformity in the iron oxide core diameter and its distribution. However, due to the finite viewing area in a TEM image, statistically significant size analysis is difficult. As a result, two methods that measure the core diameter and distribution with statistical relevance were used. In particular, magnetization curves of liquid samples (containing 100–200 μg MNPs), measured by VSM, were fit to the Langevin function to obtain the magnetic core diameter and distribution. Additionally, the peak width in powder XRD spectra was used to determine the core crystallite size.

Colloidal stability measurements

To understand the colloidal properties of MNP@PMAO-PEG, zeta potential and hydrodynamic size measurements were done using dynamic light scattering (DLS) technique (Zetasizer Nano, Malvern Instruments). For biological relevance, hydrodynamic size measurements were also made in cell culture medium. In a recent study,[39] we showed that the SLP deteriorates significantly due to reduced Brownian relaxation when MNPs dispersed in biological medium agglomerate.

Cytotoxicity study

Jurkat cells (human T-cell leukemia cell line) were grown in RPMI 1640 medium+10% fetal bovine serum (FBS) in physiological conditions (37°C and 5% CO_2). Complementary assays were conducted to confirm there is reasonable correlation between cell viability and induced toxicity. A Lactate Dehydrogenase (LDH) assay (Cytotox-ONE®, Promega) was used to determine MNP toxicity to cells by measuring LDH release in medium due to membrane disintegration. Cell viability was determined using a luciferase assay (Celltiter-GLO®, Promega), which measures ATP levels. Cells were seeded at 20,000 cells/well in a 96-well plate. MNP concentrations of 150, 300, and 450 μgFe/mL were tested for 24 h in physiological conditions. Appropriate controls were included to ensure assay validity and test for any interference MNPs or media may have with the assay. A microplate reader was used to measure fluorescence at $\lambda_{ex} = 560$ nm and $\lambda_{em} = 590$ nm for LDH assay, and a luminometer (TopCount, Perkin-Elmer) was used for measuring luminescence in the luciferase assay.

Measuring the SLP

The SLP (watts/g Fe_3O_4) as a function of MNP diameter (Table I) was measured using a dedicated hyperthermia system (magneTherm™, NanoTherics Limited, UK). The AMF frequency (f) and amplitude (H_0) were set to 373 kHz and

TABLE I. Median Diameters and Standard Deviations (σ) of As-Synthesized MNPs, Derived from Chantrell Fitting of Magnetization Curves

Median Diameter (nm)	Std. Dev. (σ)*	
	$\sigma_{avg} = 0.175$	$\sigma_{avg} = 0.284$
9	–	0.29
10	–	0.10
12	0.01	–
13	0.10	–
14	0.21	0.31
15	0.23	–
16	0.16	0.36
16.5	–	0.36
18	0.34	–

[a]The distribution of median diameters is given by the lognormal distribution function, where σ is the standard deviation.

14 kA/m respectively. A sensitive fiber-optic thermocouple (Luxtron, Lumasense Technologies) was used to measure the temperature ramp rate (dT/dt) in samples. Background temperature was averaged over 60 s and used as the baseline temperature (T_{base}), after which the AMF was turned on for 300 s. The change in temperature, ΔT ($T_{actual} - T_{base}$), was normalized for concentration (mg Fe_3O_4/mL) to graphically compare the heating rates (Fig. 1). SLP was measured using the following equation:[36]

$$\mathrm{SLP(W/gFe_3O_4)} c \frac{\mathrm{mass_{Sample}}}{\mathrm{mass_{Fe_3O_4}}} \left(\frac{dT}{dt}\right) \quad (1)$$

where c is the specific heat capacity of water (4.187 J $g^{-1}{}^{\circ}C^{-1}$), (dT/dt) is the initial slope of the heating curve (from 65 to 125 s), $mass_{sample}$ is the mass of the entire sample, and $mass_{Fe3O4}$ is mass of Fe_3O_4 in the sample determined by ICP-AES (typically ranged from 1 to 3 mg Fe_3O_4/mL). Two sets of samples (Table I) with average standard deviations (σ) of 0.175 and 0.284 were measured to specifically characterize effects of both size and size distribution on the SLP. Such characterization is intended to emphasize the significance of tailoring size to a specific frequency, thus intrinsically optimizing MFH from a material physics perspective rather than augmenting extrinsic factors such as concentration or field amplitude.

In vitro hyperthermia

Jurkat cells were cultured in triplicates at a density of 10,000 cells/well. MNPs of three sizes (12, 13, and 16 nm and σ = 0.09, 0.22, and 0.16, respectively) with varying concentrations were added to the cultured cells. Prior to AMF heating, samples and controls were incubated at 37°C for 15 min to stabilize temperature. Samples were enclosed in a thermally insulating Styrofoam™ jacket before inserting in the instrument's coil assembly. After 15 min of AMF application, cells were returned to the 37°C incubator for 15 min. Cells were allowed to equilibrate with room temperature for 30 min prior to viability measurements using the Celltiter-GLO® luciferase assay.

RESULTS

Characterization of magnetite (Fe_3O_4) MNPs

Synthesized MNPs are highly monodisperse as characterized by Transmission Electron Microscopy (TEM; FEI Tecnai™ G2 F20) imaging [Fig. 2(A)]. Hydrodynamic size of MNPs, before and after coating with PMAO-PEG, was measured using Dynamic Light Scattering (DLS). Figure 2(B) shows measurement of a 10 nm sample as an example. Magnetization curves, M(H), from VSM measurements were fit to the Langevin function, to obtain median core diameter and the volume-weighted standard deviation (σ). A lognormal distribution of particle diameter was assumed and details of the fitting method can be found in the highly cited work of Chantrell et al.[46] Unlike TEM size analysis, which provides very limited statistics of particle size distribution, the Chantrell method measures the entire sample volume, giving statistically reliable results. Median diameters and corresponding standard deviations, assuming a lognormal distribution, are shown in Table I. Magnetic properties were reconfirmed after organic to aqueous phase transfer; example of a 12 nm sample, before, after and 5 months after coating, are shown in Figure 2(D). The latter is also an indicator of the excellent shelf life of MNP@PMAO-PEG.

Powder X-ray diffraction θ–2θ scans of as synthesized MNPs are shown in Figure 3. The scans show a good match with the powder diffraction file (PDF) for magnetite (#019-0629, International Centre for Diffraction Data). As indicated in the figure, scans for MNPs of two sizes are included (top and middle). Since smaller particles (<15 nm) are nearly spherical in shape (TEM data not shown), a modified version of Scherrer's formula accounting for the spherical geometry[47] was used to determine crystal size of smaller particles (top spectrum). For quasispherical, monodisperse, and crystalline particles, the modified method shows good agreement, within 5–7%, between TEM and XRD size

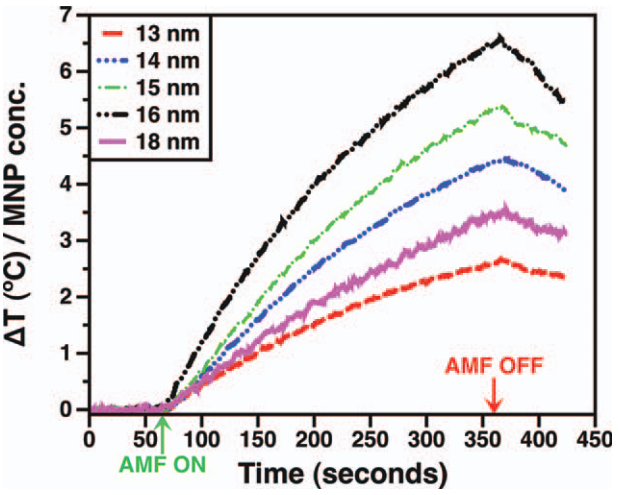

FIGURE 1. Typical heating curves of MNPs with various median diameters, obtained using a dedicated hyperthermia instrument and a fiber optic thermocouple. The temperature increase is normalized for iron oxide concentration. [Color figure can be viewed in the online issue, which is available at wileyonlinelibrary.com.]

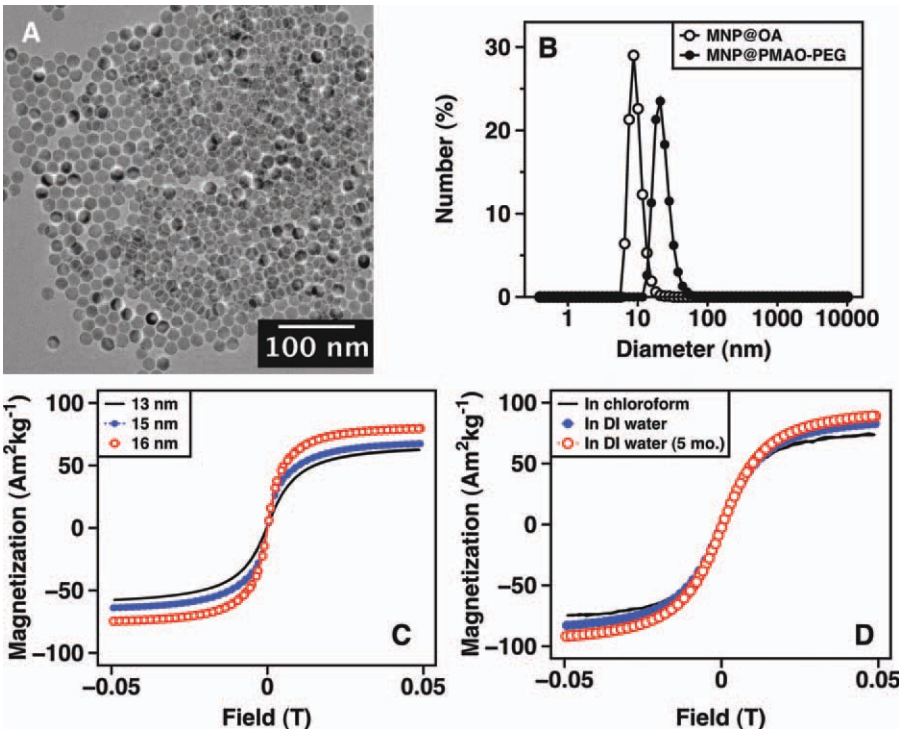

FIGURE 2. (A) TEM image of a monodisperse 16-nm sample. Because of very high monodispersity MNPs form close-packed 2D and 3D hexagonal self-assembled arrays. (B) DLS measurement of MNPs before (10 nm) and after (20 nm) phase transfer using PMAO-PEG. (C) Magnetization

measurements. The generalized form[†] was used for larger MNPs (middle scan) due to their noticeable nonspherical geometry characterized by faceting as seen in Figure 2(A). It should be noted that the generalized form of Scherrer equation can lead to ~15% error in size measurements.[47,48] The peak at 35.42° (θ = 17.71°) was chosen for all crystallite size calculations. The calculated crystal sizes are 13.7 nm and 16.9 nm for the top and middle scans, respectively. These are in good agreement with the corresponding magnetic diameters determined by the Chantrell fitting method, which are 12.9 and 15.9 nm, respectively.

Colloidal stability

MNPs preferentially disperse in the aqueous phase after coating with PMAO-PEG [Figure 4(A)] and show no signs of physical agglomeration or aggregate formation for several months. Long-term colloidal stability of MNPs in water was determined by measuring zeta potential as a function of pH [Figure 4(B)]. MNPs display a neutral surface charge across a wide range of pH values (2–12). Additionally, for biological relevance, hydrodynamic size measurements were also done in cell culture medium (RPMI 1640 + 10% FBS) to ensure MNPs remain stable during *in vitro* experiments [Figure 4(C)]. MNPs show no significant change in hydrodynamic size up to a period of 96 h of incubation in RPMI 1640 medium.

[†] $d = \frac{0.9\lambda}{W\cos\theta}$, where d is the crystal size, λ is X-ray wavelength (1.54 Å for Cu-K(α)), W is the peak width (rad) at FWHM and θ is the Bragg angle in consideration.

Cytotoxicity

Figure 5 shows results of MNP@PMAO-PEG cytotoxicity in Jurkat cells. Complementary viability (Luciferase assay) and toxicity (LDH release assay) studies were done to confirm validity of the performed assays. Cell viability drops to about 75% for the lowest concentration tested (150 μgFe/mL), while similar levels, within the calculated errors, are maintained for higher concentrations (300 and 450 μgFe/mL).

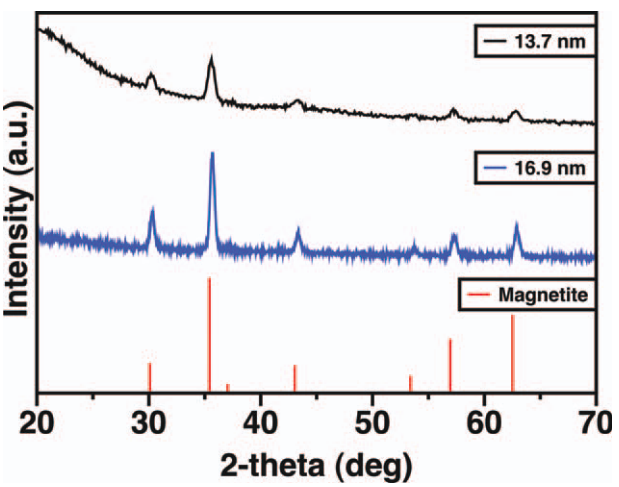

FIGURE 3. Powder X-ray diffraction, θ–2θ scans, of magnetite nanoparticles. Sizes indicated in legends were determined by Scherrer's formula using the peak at 2θ = 35.4°. The magnetite reference (bottom) was obtained from the International Centre for Diffraction Data (PDF# 019-0629). [Color figure can be viewed in the online issue, which is available at wileyonlinelibrary.com.]

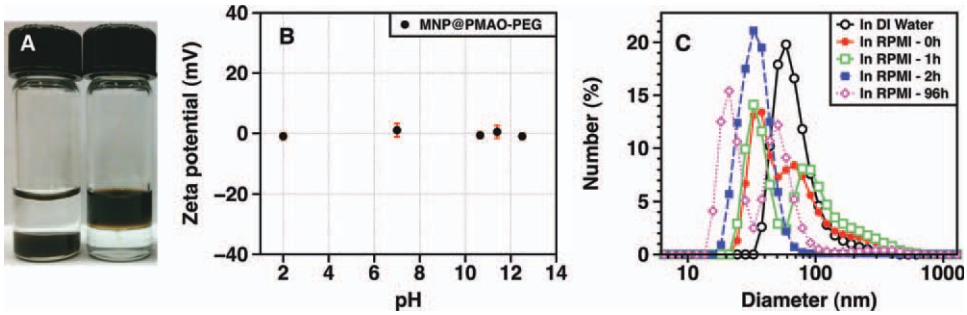

FIGURE 4. (A) MNPs preferentially disperse in the hydrophobic chloroform phase before phase transfer (left), while preferring the aqueous phase after phase transfer (right). (B) Zeta potential of MNP@PMAO-PEG as a function of pH. (C) Hydrodynamic size measurements of MNP@PMAO-PEG in RPMI 1640+10% FBS cell culture medium as a function of time. [Color figure can be viewed in the online issue, which is available at wileyonlinelibrary.com.]

The trend observed in the toxicity measurement agrees reasonably well with that observed in the viability measurement. Additionally, bright field images of cells incubated with MNPs were captured to examine any subsequent morphological alterations (Fig. 6). Jurkat cells are suspension cells and do not adhere to culture plates, as indicated by their spherical shape [Fig. 6 (A,E)]. The cellular structure and shape is consistent with the control (no MNPs) for all concentrations of MNPs [Fig. 6(B–D,F–H)].

Magnetic fluid hyperthermia

Figure 7 shows a distinct peak in SLP around 16 nm for MNPs with narrow average size distribution ($\sigma_{avg.} = 0.175$). SLP values drop by ~30% for samples with broader average size distribution ($\sigma_{avg.} = 0.284$). The drop is especially substantial for 16-nm particles.

These experimental results were compared with a theoretical model for optimizing magnetic hyperthermia, rigorously developed by Carrey et al.[38] According to this model, the optimum volume (V_{opt}) for randomly oriented MNPs is given by:

$$V_{opt} = \frac{-k_B T \ln(\pi f \tau_0)}{K_{eff}\left(1 - \frac{1.69\mu_0 H_{max} M_s}{2K_{eff}}\right)^{\frac{4}{3}}} \quad (2)$$

where, k_B = Boltzmann constant (1.38×10^{-23} J K^{-1}), T = temperature (300 K), f = applied field frequency (kHz),

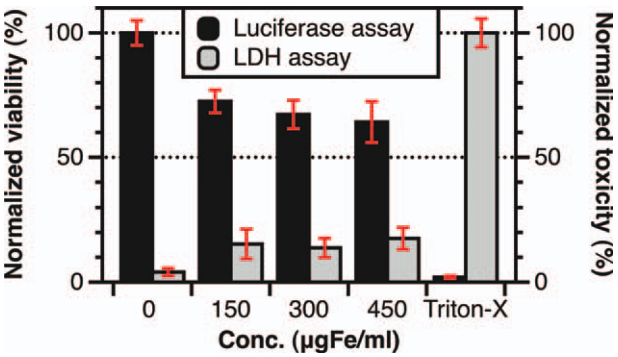

FIGURE 5. *In vitro* cytotoxicity of MNP@PMAO-PEG in Jurkat cells. Viability measured via Luciferase assay and toxicity measured via LDH assay. MNPs were incubated for 24 h in physiological conditions (37°C and 5% CO_2). [Color figure can be viewed in the online issue, which is available at wileyonlinelibrary.com.]

τ_0 = attempt time (~10^{-10} s), K_{eff} = anisotropy constant (23–41 kJ m^{-3})[37], $\mu_0 H_{max}$ = field amplitude ($4\pi \times 10^{-7}$ H m^{-1} × H_{max} kA m^{-1}), and M_s = saturation magnetization (450 kA m^{-1}).[49] Depending on the anisotropy constant of magnetite, for an AMF with f = 373 kHz and H_{max} = 14 kA m^{-1}, the optimum diameter ($D_{opt} = [6 \times V_{opt}/\pi]^{1/3}$) can range from 13 nm (for K_{eff} = 40 kJ m^{-3}) to 17 nm (for K_{eff} = 23 kJ m^{-3}). Our experimental result showing 16 nm as the peak diameter falls within this range and confirms well with the model. Although such a model is useful for identifying the optimum size range for magnetic nanoparticles under fixed field conditions, it is important to note that at the nanoscale, the anisotropy constant varies significantly from bulk values due to shape[19] and surface[50] contributions to the magnetocrystalline anisotropy.

In vitro hyperthermia

In order to study the *in vitro* effect of magnetic fluid hyperthermia, ATP levels in Jurkat cells, as a measure of metabolic activity or cell viability, were compared. Although the controls (no MFH) experienced small declines in viability as a function of MNP concentration, due to some minor toxicity from potential organic residues in the phase transfer, cells exposed to MFH showed distinctly greater decrease in viability compared with controls (Fig. 8). More importantly, since the goal of this study is to emphasize the intrinsic optimization of MFH by size tailoring, monodisperse MNPs of three different diameters were compared. Totally, 16 nm (σ = 0.16) MNPs, the optimal size for our chosen AMF as per the maximum observed in SLP measurements (Fig. 6), were compared with 12 (σ = 0.09) and 13 (σ = 0.22) nm MNPs. The decrease in viability, relative to control, is markedly greater for the 16 nm MNPs compared with 12 and 13 nm MNPs (Fig. 9). Also note, MNP concentration is slightly lower for 16 nm sample compared with 12 and 13 nm samples[‡].

DISCUSSION

The heat generated by magnetic particles when subject to an AMF, which forms the basis of MFH, depends on two parameters: the applied frequency, f, and one that is

[‡]Due to technical problems with the ICP-AES, concentration of the 16 nm sample was rechecked and corrected. This explains the concentration difference between the 16 nm and the 12 and 13 nm samples.

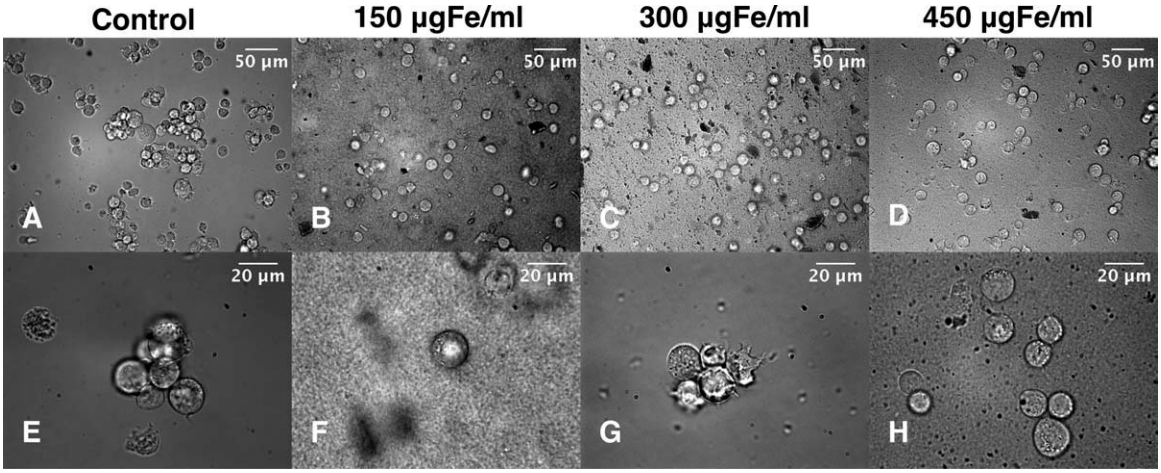

FIGURE 6. Bright field images of Jurkat cells after 24-h incubation with MNP@PMAO-PEG. Images A–D were taken at ×20 and E–H at ×60 magnification, respectively.

intrinsic to the magnetic properties of the nanoparticle, that is their relaxation time, τ. The relaxation time can be either Néel, which depends exponentially on the magnetic core volume, or Brownian, which depends linearly on the hydrodynamic volume. The faster process dominates the relaxation time and for the sizes (particles exhibiting superparamagnetism at room temperature) and frequencies of interest in MFH, the Néel relaxation time is predominant. Thus the heating of superparamagnetic MNPs in MFH applications depends critically on matching the nanoparticle size to the applied frequency and more importantly, keeping their size distribution as narrow as possible. Specifically, from the perspective of clinical application, to minimize dose and time of application for the required therapeutic outcome, the relatively modest magnetic characteristics of Fe_3O_4 MNPs require utmost optimization of the material parameters (size, size distribution, shape, phase purity, defect free) responsible for enhancing MFH. The extremely stringent criteria discussed here, and the fact that truly monodisperse MNPs can only be reproducibly synthesized via organic routes in toxic organic solvents, demands the need for a thorough physical, chemical, and cytotoxicity characterization.

TEM [Fig. 2(A)] and XRD (Fig. 3) analysis show that the Fe_3O_4 MNPs are highly monodisperse and single phase, respectively. Additionally, magnetic properties of MNPs are superior, with saturation magnetization reaching as high as 75 A m^2 kg^{-1} for 16 nm MNPs [Fig. 2(C)], that is, ~83% of bulk saturation value for magnetite (~90 A m^2 kg^{-1}). Because of the presence of ~0.5 nm layer of disordered spins on the surface of the MNPs that do not contribute to the total saturation magnetization of the sample, superparamagnetic particles often have lower saturation values compared to bulk.[50] It also explains why the crystalline diameter, determined from XRD spectrum (Fig. 3), is ~1 nm larger than the magnetic core diameter, determined by the Chantrell method. After transfer from the organic to the aqueous phase using the amphiphilic PMAO-PEG polymer, MNPs show exceptional stability in water [up to a year, Fig. 4(A)] and retain their superior magnetic properties up to the tested period of 5 months [Fig. 2(D)]. The magnetic core diameters as determined using the Chantrell method confirm MNPs remain nearly monodisperse even after phase transfer (Table I), suggesting no aggregation during the phase transfer process. Zeta potential as a function of pH shows MNPs display a near neutral surface charge across a wide pH range (2–12). This suggests MNPs are primarily stabilized via steric repulsion due to the surface PEG layer, and are less prone to adsorption form charged proteins or, in general, nonimmunogenic. Hydrodynamic size measurements performed in cell culture medium [Fig. 4 (C)] emphasize the biological relevance. To elucidate this further, in a recent study[39] we showed that MNPs can exhibit a combination of Néel (moment reversal) and Brownian (particle reversal) relaxation if the size lies within the Néel to Brownian transition.[37] Thus, for particles agglomerating in culture medium, the Brownian component of the relaxation, which depends on the hydrodynamic volume, is essentially blocked, decreasing the overall SLP output. MNP@PMAO-PEG are relatively stable for up to 96 h in RPMI 1640 + 10% FBS cell culture

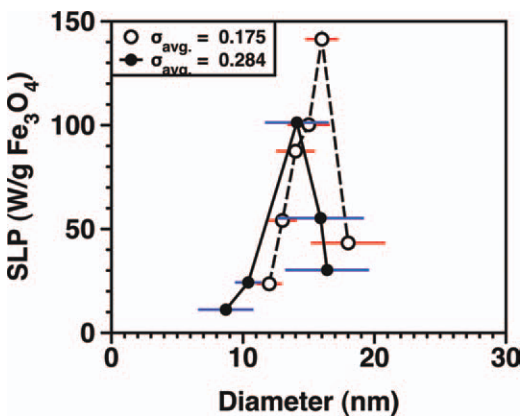

FIGURE 7. Specific loss power (W/g Fe_3O_4) as a function of size and size distribution. Frequency (f) = 373 kHz and H_o = 14 kA/m. [Color figure can be viewed in the online issue, which is available at wileyonlinelibrary.com.]

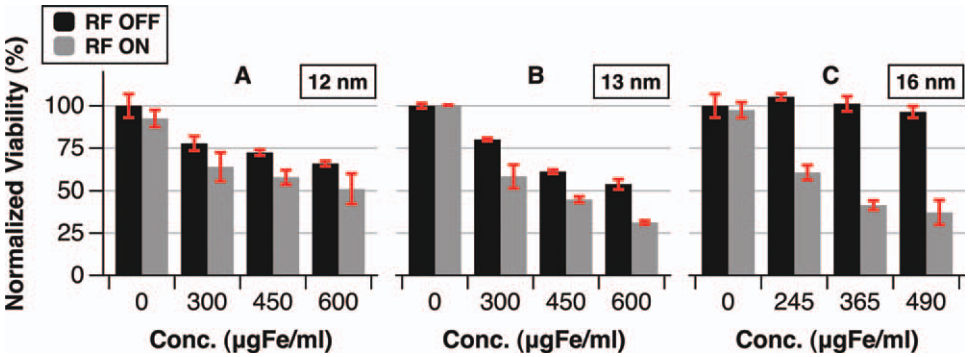

FIGURE 8. *In vitro* heating of Jurkat cells using MNPs of median diameters (A) 12 nm, (B) 13 nm, and (C) 16 nm. AMF was applied for 15 min. [Color figure can be viewed in the online issue, which is available at wileyonlinelibrary.com.]

medium [Fig. 4 (C)], suggesting consequent decrease in SLP output due to particle agglomeration is not expected.

Cytotoxicity results confirm MNPs exhibit relatively low inherent toxicity in Jurkat cells (Fig. 5). Typically, the total amount of iron stores in the human body is ~3500 mg and the total amount of iron oxide used for diagnostic imaging is relatively small (~5.6 μgFe/mL).[51] The maximum concentration used in our cytotoxicity experiments (up to 450 μgFe/mL) is far greater than the actual *in vivo* use. This ensures that we are measuring for cytotoxicity beyond current clinically tried levels. Overall, both viability and toxicity assays complement each other reasonably well, within the calculated error. Bright field images of cells (Fig. 6) at 20× and 60× magnification confirm that overall cell morphology is preserved after 24 h of incubation with MNPs of various concentrations.

Our comprehensive experimental SLP data as a function of both size and size distribution (Fig. 7) shows that, for the chosen AMF conditions (373 kHz and 14 kA/m), 16 nm monodisperse MNPs exhibit the optimum SLP. More importantly, a clear peak in the heating as a function of MNP size is demonstrated. Additionally, MNPs with broader average size distributions show an overall drop in the peak SLP value. The drop is especially dramatic at 16 nm, which is the peak maximum for samples with narrow average distributions. This is consistent with theoretical models that show significant degradation of heating rates at or near the optimum size compared with nonoptimum sizes. As a result, with broader average distribution the peak appears to shift to a lower median size (14 nm), when in fact, it is broadening and flattening out near the maximum. The experimental data presented here also provides strong validity to theoretical models of MFH,[2,37] especially the need for size-tuned, monodisperse MNPs for maximizing SLP.

The *in vitro* therapeutic efficacy of MFH to induce cell death has been rigorously demonstrated in heating experiments with Jurkat cells as a function of both MNP concentration and, most critically, size (Figs. 8 and 9). As expected, increasing MNP concentration increases heating rates; consequently reduction in % viability is also enhanced (Fig. 8). As described earlier, enhancing MFH by increasing MNP concentration, which is an extrinsic parameter, does not indicate an improvement in the overall therapeutic potency of MFH. The key result, however, is the significant decrease in % viability due to the optimum 16-nm sized MNPs compared with the 12 and 13 nm MNPs under the same AMF conditions. This result (Fig. 9) underscores the central idea of tailoring size for a specific frequency in order to intrinsically improve the therapeutic potency of MFH.

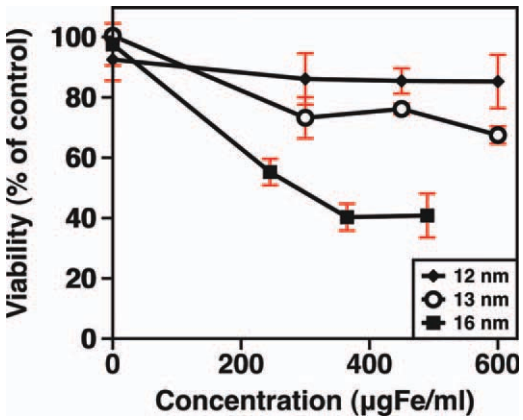

FIGURE 9. Cell viability relative to control calculated as AC $OFF_{avg.}$ – AC $ON_{avg.}$ [Color figure can be viewed in the online issue, which is available at wileyonlinelibrary.com.]

CONCLUSION

We have shown with systematic experiments that magnetite MNPs, with optimal magnetic properties and tailored to a specific alternating magnetic field frequency (f = 373 kHz) can show significant enhancement in MFH. Specifically, a peak in the heating rate or SLP as a function of MNP diameter has been clearly demonstrated and *in vitro* heating shows that optimized MNPs (16 nm) and narrow size distributions (a 30% difference in SLP is observed between σ–0.175 and σ–0.284) have maximum efficiency in reducing cell viability, suggesting our SLP data translates truthfully to cell populations. All this is achieved by synthesizing monodisperse MNPs via organic synthesis routes and successfully transferring them to aqueous phase using a biocompatible amphiphilic polymer. A rigorous characterization protocol, described in detail, ensures that the MNPs meet all the critical requirements: (1) uniform shape and monodispersity,

(2) phase purity, (3) stable magnetic properties approaching that of the bulk, (4) colloidal stability, (5) substantial shelf life, and (6) pose no significant *in vitro* toxicity. Finally, the conclusions are general and present a way to tailor/synthesize optimal, biocompatible MNPs for MFH at any applied frequency.

REFERENCES

1. Edwards BK, Ward E, Kohler BA, Eheman C, Zauber AG, Anderson RN, Jemal A, Schymura MJ, Lansdorp-Vogelaar I, Seeff LC, van Ballegooijen M, Goede SL, Anderson R, Ries LAG. Annual report to the nation on the status of cancer, 1975–2006, featuring colorectal cancer trends and impacts of interventions (risk factors, screening, and treatment) to reduce future rates. Cancer Cytopathol 2009;116:544–573.
2. Krishnan KM. Biomedical nanomagnetics: A spin through possibilities in imaging, diagnostics, and therapy. IEEE T Magn 2010; 46:2523–2558.
3. Gupta AK, Gupta M. Synthesis and surface engineering of iron oxide nanoparticles for biomedical applications. Biomaterials 2005;26:3995–4021.
4. Montet X, Funovics M, Montet-Abou K, Weissleder R, Josephson L. Multivalent Effects of RGD peptides obtained by nanoparticle display. J Med Chem 2006;49:6087–6093.
5. Hafeli UO, Riffle JS, Harris-Shekhawat L, Carmichael-Baranauskas A, Mark F, Dailey JP, Bardenstein D. Cell uptake and in vitro toxicity of magnetic nanoparticle suitable for drug delivery. Mol Pharm 2009;6:1417–1428.
6. Pankhurst QA, Thanh NKT, Jones SK, Dobson J. Progress in applications of magnetic nanoparticles in biomedicine. J Phys D Appl Phys 2009;42:22401.
7. Weissleder R, Cheng H-C, Bogdanova A, Bogdanova A. Jr. Magnetically labeled cells can be detected by MR imaging. JMRI-J Magn Reson Im 1997;7:258–263.
8. Gleich B, Weiznecker J. Tomographic imaging using the nonlinear response of magnetic particles. Nature 2005;435:1214–1217.
9. Ferguson M, Khandhar A, Minard K, Krishnan KM. Optimizing magnetite nanoparticles for mass sensitivity in magnetic particle imaging. Med Phys 2011;38:1619–1626.
10. Dobson J. Gene therapy progress and prospects: Magnetic nanoparticle-based gene delivery. Gene Ther 2006;13:283–287.
11. Danhier F, Vroman B, Lecouturier N, Crokart N, Pourcelle V, Freichels H, Jérôme C, Marchand-Brynaert J, Feron O, Préat V. Targeting of tumor endothelium by RGD-grafted PLGA-nanoparticles loaded with paclitaxel. J Control Release 2009;140:166–173.
12. Byrne JD, Betancourt T, Brannon-Peppas L. Active targeting schemes for nanoparticle systems in cancer therapeutics. Adv Drug Deliver Rev 2008;60:1615–1626.
13. Haley B, Frenkel E. Nanoparticles for drug delivery in cancer treatment. Urol Oncol-Semin ORI 2008;26:57–64.
14. Hahn GM. Hyperthermia for the engineer: A short biological primer. IEEE T Bio-Med Eng 1984;311:3–8.
15. Hildebrandt B, Wust P, Ahlers O, Dieing A, Sreenivasa G, Kerner T, Felix R, Riess H. The cellular and molecular basis of hyperthermia. CRC Cr Rev Oncol-Hem 2002;42:33–56.
16. Henle KJ, Leeper DB. Interaction of hyperthermia and radiation in CHO cells: Recovery kinetics. Radiat Res 1976;66:505–518.
17. Marmor JB. Interactions of hyperthermia and chemotherapy in animals. Cancer Res 1979;39:2269–2276.
18. Sun S, Murray CB. Synthesis of monodisperse cobalt nanocrystals and their assembly into magnetic superlattices (invited). J Appl Phys 1999;85:4325–4330.
19. Krishnan KM, Pakhomov AB, Bao Y, Blomqvist P, Chun Y, Gonzales M, Griffin K, Ji X, Roberts BK. Nanomagnetism and spin electronics: Materials, microsctructure and novel properties. J Mater Sci 2006;41:793–815.
20. Bao Y, Beerman M, Pakhomov AB, Krishnan KM. Controlled crystalline structure and surface stability of cobalt nanocrystals. J Phys Chem B 2005;109:7220–7222.
21. Sun S. Recent advances in chemical synthesis, self-assembly, and applications of FePt nanoparticles. Adv Mater 2006;18:393–403.
22. Gonzales M, Mitsumori LM, Kushleika JV, Rosenfeld ME, Krishnan KM. Cytotoxicity of iron oxide based nanoparticles made from the thermal decomposition of organometallics and aqueous phase transfer with Pluronic F127. Contrast Media Mol I 2010;5:286–293.
23. Weissleder R, Stark DD, Engelstad BL, Bacon BR, Compton CC, White DL, Jacobs P, Lewis J. Superparamagentic iron oxide: Pharmacokinetics and toxicity. Am J Roentgenol 1989;152:167–173.
24. Tiefenauer LX. Magnetic nanoparticles as contrast agents for medical diagnosis. In: Vo-Dinh T, editor. Nanotechnology in Biology and Medicine. Boca Raton: Taylor & Francis Group LLC; 2007. p 1–20.
25. Lu M, Cohen MH, Rieves D, Pazdur R. FDA Report: Ferumoxytol for intravenous iron therapy in adult patients with chronic kidney disease. Am J Hematol 2010;85:315–319.
26. Tartaj P, Morales MP, Veintemillas-Verdaguer S, Gonzales-Carreño, Serna CJ. Synthesis, properties and biomedical applications of magnetic nanoparticles. In: Buschow KHJ, editor. Handbook of Magnetic Materials Volume 16. Amsterdam: Elsevier BV; 2006. pp 403–482.
27. Bao Y, Krishnan KM. Preparation of functionalized cobalt nanocrystals for potential biomedical applications. J Magn Magn Mater 2005;293:15–19.
28. Bao Y, Calderon H, Krishnan KM. Synthesis and characterization of magnetic-optical Co-Au core-shell nanoparticles. J Phys Chem 2007;C111:1941–1944.
29. Fortin J-P, Gazeau F, Wilhelm C. Intracellular heating of living cells through Néel relaxation of magnetic nanoparticles. Eur Biophys J 2008;37:223–228.
30. Hilger I, Kießling A, Romanus E, Hiergeist R, Hergt R, Andra W, Roskos M, Linss W, Weber P, Weitschies W, Kaiser WA. Magnetic nanoparticles for selective heating of magnetically labeled cells in culture: preliminary investigation. Nanotechnology 2004;15: 1027–1032.
31. Jordan A, Scholz R, Wust P, Schirra H, Schiestel T, Schmidt H, Felix R. Endocytosis of dextran and silan-coated magnetite nanoparticles and the effect of intracellular hyperthermia on human mammary carcinoma cells in vitro. J Magn Magn Mater 1999;194: 185–196.
32. Hou C-H, Chen C-W, Hou S-M, Li Y-T, Lin F-H. The fabrication and characterization of dicalcium phosphate dihydrate-modified magnetic nanoparticles and their performance in hyperthermia processes in vitro. Biomaterials 2009;30:4700–4707.
33. Hilger I, Hergt R, Kaiser WA. Use of magnetic nanoparticle heating in the treatment of breast cancer. IEE P-Nanobiotechnol 2005; 152:33–39.
34. Ivkov R, DeNardo J, Daum W, Foreman AR, Goldstein RC, Valentin SN, DeNardo GL. Application of high amplitude alternating magnetic fields for heat induction of nanoparticles localized in cancer. Clin Cancer Res 2005;11:7093s–7103s.
35. Giering K, Lamprecht I, Minet I, Handke A. Determination of the specific heat capacity of healthy and tumorous human tissue. Thermochim Acta 1995;251:199–205.
36. Gonzales-Weimuller M, Zeisberger M, Krishnan KM. Size-dependent heating rates of iron oxide nanoparticles for magnetic fluid hyperthermia. J Magn Magn Mater 2009;321:1947–1950.
37. Rosensweig RE. Heating magnetic fluid with alternating magnetic field. J Magn Magn Mater 2002;252:370–374.
38. Carrey J, Mehdaoui, Respaud M. Simple models for dynamic hysteresis loop calculations of magnetic simple-domain nanoparticles: Application to magnetic hyperthermia optimization. J Appl Phys 2011;109:083921.
39. Khandhar AP, Ferguson RM, Krishnan KM. Monodispersed magnetite nanoparticles optimized for magnetic fluid hyperthermia: Implications in biological systems. J Appl Phys 2011;109:07B310.
40. Kawashita M, Tanaka M, Kokubo T, Inoue Y, Yao T, Hamada S, Shinjo T. Preparation of ferromagnetic magnetite microspheres for in situ hyperthermia treatment of cancer. Biomaterials 2005;26: 2231–2238.
41. Jana NR, Chen Y, Peng X. Size- and shape-controlled magnetic (Cr, Mn, Fe, Co, Ni) oxide nanocrystals via a simple and general approach. Chem Mater 2004;16:3931–3935.
42. Kalale S, Narain R, Krishnan KM. Probing temperature-sensitive behavior of pNIPAA-m coated iron oxide nanoparticles using

frequency-dependent magnetic measurements. J Magn Magn Mater 2009;321:1377–1380.
43. Narain R, Gonzales M, Hoffman AS, Stayton PS, Krishnan KM. Synthesis of monodisperse biotinylated p(NIPAAm)-coated iron oxide magnetic nanoparticles and their bioconjugation to streptavidin. Langmuir 2007;23:6299–6304.
44. Mengast A, Ferguson RM, Khandhar AP, Grogger W, Hofer F, Krishnan KM. unpublished.
45. Klibanov AL, Maruyama K, Beckerleg AM, Torchilin VP, Huang L. Activity of amphiphatic poly(ethylene glycol) 5000 to prolong the circulation time of liposomes depends on the liposome size and is unfavorable for immunoliposome binding to target. Biochim Biophys Acta 1991;1062:142–148.
46. Chantrell RW, Popplewell J, Charles SW. Measurements of particle size distribution parameters in ferrofluids. IEEE T Magn 1978; 14:975–977.
47. Borchert H, Shevchenko EV, Robert A, Merkix I, Kornowski A, Grübel G, Weller H. Determination of nanocrystal sizes: A comparison of TEM, SAXS, and XRD studies of highly monodisperse $CoPt_3$ particles. Langmuir 2005;21:1931–1936.
48. Patterson AL. The Scherrer formula for X-ray particle size determination. Phys Rev 1939;56:978–982.
49. Cornell RM, Schwertmann U. The Iron Oxides: Structures, Properties, Reactions, Occurrence and Uses. New York: Weinheimm; 1996.
50. Pal S, Dutta S, Shah N, Huffman GP, Seehra MS. Surface spin disorder in fe_3o_4 nanoparticles probed by electron magnetic resonance spectroscopy and magnetometry. IEEE T Magn 2007;43: 3091–3093.
51. AMAG Pharmaceuticals: Available at: www.amagpharma.com/products/feridex_iv.php. Feridex I.V. ® Package Insert. Revised May 2007.